Neural code subserving feed-forward inhibition in a collision detection circuit

Hongxia Wang[1], Richard B. Dewell[1], Ying Zhu[1, 2], Fabrizio Gabbiani[1, 2, 3,*]

[1]Department of Neuroscience, Baylor College of Medicine, Houston, TX

[2]Quantitative and Computational Biosciences, Graduate Program, Baylor College of Medicine, Houston, TX

[3]Electrical and Computer Engineering Department, Rice University, Houston, TX

*Correspondence: gabbiani@bcm.edu

Summary

Feed-forward inhibition shapes the activity of many neural circuits, although little is known about how (and even if) neurons mediating feed-forward inhibition encode detailed time-varying sensory information. Locusts possess an identified neuron preferentially responding to objects approaching on a collision course that plays a central role in the generation of visually-guided escape behavior. This neuron, called the Lobula Giant Movement Detector (LGMD), receives both feed-forward excitation and inhibition. While feed-forward excitation encodes a function of the angular speed of expansion during the simulated approach of an object, the information conveyed by feed-forward inhibition remains to be characterized. We identified presynaptic, inhibitory neurons to the LGMD using spike-triggered membrane potential averaging. Unexpectedly, these neurons had wide receptive fields and only a small population of them was needed to account for most of the information they conveyed to the LGMD. Together, the time-varying spike rate of these neurons accurately encoded the instantaneous angular size of an approaching object. Our results show that feed-forward inhibitory neurons convey detailed information about a stimulus parameter needed to generate escape behaviors, and thus likely play a critical role in their timing.

Introduction

Within neural networks, inhibition operates in close concert with excitation to shape the computations and firing properties of individual neurons. Inhibition is often subdivided in three types, thought to possess distinct computational properties: feed-forward, lateral and feedback (recurrent). Feedback inhibition, e.g., from layer 2/3 interneurons onto pyramidal cells in cortex, has been shown to adjust the sensitivity and transfer function of neural circuits (Fino and Yuste, 2011; Kapfer et al., 2007). Lateral inhibition sharpens neuronal tuning in a variety of topographic mappings, by providing surround suppression (e.g., Wu et al., 2008; Ozeki et al., 2009; Norton et al., 1989). Feed-forward inhibition enhances the temporal fidelity of single neurons, including Purkinje and pyramidal cells (Mittmann et al., 2005; Pouille and Scanziani, 2001; Gabernet et al., 2005; Blitz and Regehr, 2005). In invertebrates, feed-forward inhibition has also been shown to sharpen the responses of mushroom body Kenyon cells to odors (Perez-Orive et al., 2002) and is required for appetitive memory expression in *Drosophila* (Perisse et al., 2016). Yet, we

still don't know if such feed-forward inhibitory neurons convey detailed time-varying information beyond their well-documented temporal sharpening and synchronizing effects on information conveyed by feed-forward excitation.

The lobula giant movement detector (LGMD) in the locust optic lobe is a well-studied identified neuron (O'Shea and Williams 1974), selectively responding to objects approaching on a collision course or their two-dimensional simulation on a screen (looming stimuli; Schlotterer, 1977; Rind and Simmons, 1992; Hatsopoulos et al., 1995). The LGMD receives both feed-forward excitatory and inhibitory inputs from neurons in the second visual neuropil, the medulla, and conveys its spiking output to a postsynaptic identified pre-motor neuron, the descending contralateral movement detector (DCMD; Rind, 1984). Feed-forward excitation impinges on one dendritic field of the LGMD and is sculpted by a range of presynaptic mechanisms, including lateral excitation, lateral inhibition and normalizing inhibition (O'Shea and Rowell, 1975a; Rowell et al., 1977; Zhu et al., 2017). Feed-forward inhibition is subdivided in two distinct channels which sense ON (luminance increments) and OFF (luminance decrements) transients and impinges on two additional dendritic fields (Rowell et al., 1977; Gabbiani et al., 2002, 2005). The activation of feed-forward inhibition has been proposed to help terminate the LGMD's response to looming stimuli (Hatsopoulos et al., 1995; Gabbiani et al., 1999, 2002), a process thought to be critical to the generation of escape behaviors (Fotowat et al., 2011). However, little is currently known about the medullary neurons presynaptic to the LGMD mediating feed-forward inhibition. In the locust medulla, non-directional, columnar motion-sensitive neurons with small receptive fields have been characterized (e.g., Osorio, 1991; James and Osorio, 1996), as well as tangential neurons with wider receptive fields but similar overall characteristics (Homberg and Würden, 1997).

To investigate the neurons contributing to feed-forward inhibition in this collision detection circuit and their coding properties, we carried out in vivo sharp electrode intracellular recordings from the LGMD and simultaneous extracellular recordings from putative inhibitory medullary neurons to study their connections with the LGMD. Using moving edges and looming stimuli simulating the approach of an object at constant velocity, we studied the visual receptive fields and characterized the response properties of those neurons identified to be presynaptic to the LGMD. We found that such neurons have wide receptive fields and exert inhibition through $GABA_A$ receptors. Interestingly, their firing pattern resembled that of the LGMD, gradually increasing, peaking and decaying towards the time of collision. Because the firing rate of the LGMD in response to looming stimuli can be described by the multiplication of the angular speed of an approaching object with a negative exponential of its angular size, this suggested that feed-forward inhibition might code for some function of angular size (Gabbiani et al., 2002). Excitation had been characterized and shown to encode a function of angular speed (Jones and Gabbiani, 2012). The electrophysiological recordings reported here allowed us to test whether the firing rate of inhibitory medullary neurons presynaptic to the LGMD encodes the angular size or speed of looming stimuli or functions of them. Our results demonstrate that feed-forward inhibition conveys time-varying information about an approaching object's size, in parallel to the speed information conveyed by feed-forward excitation, which likely plays a critical role in timing of the LGMD's output and

associated escape behaviors.

Results

Feed-forward inhibition mediated by DUB medullary afferents and postsynaptic $GABA_A$ receptors significantly reduces the LGMD's excitability.

As illustrated in Fig. 1A, the LGMD neuron possesses three dendritic fields, labeled A, B and C. Dendritic field A receives retinotopically organized, motion-sensitive excitatory inputs from an entire visual hemifield. These inputs are provided by a columnar projection originating at the ommatidia (facets) of the compound eye lattice (Peron et al., 2009; Zhu and Gabbiani, 2016). The axons of columnar retinotopic neurons mediating these inputs form two optic chiasms. The first one is located between the lamina and the medulla (Fig. 1B), and the second one between the medulla and the lobula. In these chiasms axons cross the midline resulting in an inversion of the visual world about the sagittal plane. Dendritic field C, on the other hand, receives inputs thought to mediate inhibition to transient light OFF stimuli (Rowell et al., 1977). Consistent with this hypothesis, puffing the $GABA_A$ blocker picrotoxin onto dendritic field C increases and prolongs responses to visual stimuli (Gabbiani et al., 2002, 2005). Anatomical and electrophysiological evidence suggests that these inhibitory inputs are mediated by ~500 axons originating in the medulla and forming an uncrossed (non-inverting) axonal tract called the dorsal uncrossed bundle (DUB, Fig. 1B; Rowell et al., 1977; Strausfeld and Nassel, 1981; Elphick et al., 1996).

To study the input from medullary neurons in the DUB to the LGMD, we inserted an intracellular electrode in dendritic field C of the LGMD and a pair of extracellular electrodes (stereotrode) at a distance of ~200 μm on the dorsal aspect of the lobula, where the DUB lies (Fig. 1C). First we confirmed that dendritic field C receives inhibitory inputs by puffing GABA close to dendritic field C and monitoring the membrane potential (V_m) of the LGMD in response to looming stimuli. We used stimuli with a half-size to speed ratio $l/|v|$ = 40 ms, where l represents the half-size of the approaching object, and v its translation speed towards the locust eye (Fig. 1D, inset). The responses of the LGMD are depicted in Figs. 1D and E. As the simulated object approaches the locust eye, its angular size (θ) increases nearly exponentially and the LGMD firing rate gradually increases, peaks and finally decays towards the time of collision (t = 0), consistent with previous results (Gabbiani et al., 2002, 2005). Compared with the control response, GABA application significantly reduced the number of spikes emitted by the LGMD and the magnitude of its instantaneous firing rate, as well as its mean over the entire trial (Figs. 1D and E). In some trials, GABA application (~300 μM; Methods) could even abolish all the spikes normally induced by looming stimuli. Additionally, in the first trial following GABA application, we found the membrane potential of the LGMD to be tonically hyperpolarized by 2.9 ± 2.4 mV (mean ± s.d., n = 5 animals, average over 1 s before stimulus onset, p = 0.0312, one-sided sign-rank test). Over a total of five successive trials, the membrane potential remained hyperpolarized, albeit at a slightly less pronounced level, 2.1 ± 2.3 mV (p = 0.0625, one-sided sign-rank test). These results indicate that $GABA_A$ receptor mediated inhibition to dendritic field C of the LGMD is

involved in mediating feed-forward inhibition to the LGMD. Further, the effects of GABA application are consistent with previous findings that the $GABA_A$ receptor blocker picrotoxin enhanced the LGMD's responses to looming stimuli (Gabbiani et al. 2002, 2005). Next, we verified the positioning of our extracellular electrodes in the DUB by bipolar electrical stimulation during the presentation of looming stimuli. Electrical stimulation elicited a tightly coupled compound IPSP in the LGMD that transiently inhibited its spiking response (Fig. 1F). The membrane hyperpolarization evoked by electrical stimulation during the looming response amounted to -13.58 ± 3.05 mV and could be reliably detected within the LGMD spiking discharge at an earliest detectable latency of 3.38 ± 0.61 ms (n = 7; Methods). In contrast, we confirmed that stimulation outside the DUB elicited excitatory responses in the LGMD in another set of electrical stimulation experiments paired with intracellular LGMD recordings (Supp. Fig. 1). In these experiments, the membrane hyperpolarization following the initial EPSP evoked by electrical stimulation in the DUB amounted to -4.25 ± 1.53 mV with an earliest detectable latency of 4.58 ± 0.90 ms (n = 6). These results agree with a previous characterization of OFF inhibition to dendritic field C of the LGMD (Rowell et al., 1977).

Identification of presynaptic inhibitory input neurons to LGMD's dendritic field C.

Fig. 2A (top panel) shows spontaneous activity recorded extracellularly in the DUB along the dorsal edge of the lobula, close to the location of dendritic field C. The bottom trace is a simultaneous intracellular recording from dendritic field C. A close-up view of this trace reveals that the V_m in dendritic field C exhibits both spontaneous excitatory and inhibitory postsynaptic potentials at the resting membrane potential of -63 mV (sEPSPs and sIPSPs, respectively; Fig. 2A, black and gray arrowheads in inset), resulting in a membrane noise of 0.72 mV (average s.d. of V_m, n = 10 animals) lower than that observed in dendritic field A (s.d. = 1.05 mV; Jones and Gabbiani 2012). Although the extracellular trace clearly contains several units, as can be deduced from variable spike amplitudes, their relation to the LGMD's V_m is not obvious because it was difficult to discern a direct temporal V_m change in the LGMD following individual medullary spikes.

To distinguish different units of the DUB, we performed spike sorting on the extracellular recordings using principal component analysis followed by K-means clustering and identified 3 to 4 well isolated clusters per experiment (Fig. 2B; see Methods). Spike waveforms consisted of 31 sample points and had different sizes and shapes on the two electrodes (Fig. 2C). Next, we performed spike-triggered averages of the LGMD membrane potential separately for the spikes in each cluster and determined that some units (typically 2-3) were associated with transient hyperpolarizations of its V_m. In the example illustrated in Fig 2D, two clusters exhibit such spike-triggered transient hyperpolarizations (Fig. 2D, *) that resembled inhibitory post-synaptic potentials (IPSPs), while the third cluster did not reveal any associated V_m change above the noise threshold level (Fig. 2D, dashed lines). The spike-triggered hyperpolarization events disappeared after randomization of the LGMD V_m trace relative to the spikes of each cluster, confirming that they were associated with specific clusters (Supp. Fig. 2A). Additionally, such transient hyperpolarizations could be detected in the inhibitory dendritic branches of

field C, but not during intracellular recordings in the excitatory dendritic field. These transient hyperpolarizations, however, were not chemical IPSPs for at least three reasons. First, the duration of the hyperpolarization was short, < 1 ms, unlike $GABA_A$ mediated synaptic potentials, which typically last several milliseconds or more. Second, they were usually preceded by smaller transient depolarizations (Fig. 2D, green and orange arrowheads) and sometimes followed by a rebound (top trace in Fig. 2D, grey arrowhead). Third, the latency of their peak (Fig. 2D, *) with respect to the extracellular spike peak (dashed blue line in Fig. 2D) was very short, < 0.3 ms. To confirm this point, we plotted the distribution of trough times across all clusters in all experiments and found a median value of 0.05 ms (Fig. 2E, dashed red line). These observations suggested that the spike-triggered transients might be mediated by electrical synapses and could thus correspond to an attenuated version of the presynaptic neuron's action potentials.

To further investigate this point, we plotted single examples of extracellularly recorded spikes scaled to match the transient V_m hyperpolarization following them (Fig. 2F, left) and repeated this procedure after averaging over hundreds of them (Fig. 2F, right). We noted that shifting the extracellular spike by ~0.45 ms yielded a good match between its shape and that of the transient hyperpolarization, both before and after averaging (Fig. 2F, dashed lines). This suggests that the initial rapid phase of the pre-synaptic action potential corresponds to the initial V_m depolarization observed in Fig. 2F (black and green arrowheads, respectively) and that it is further attenuated due to its higher frequency content than the following after-hyperpolarization phase corresponding to the second, slower phase of the extracellularly recorded action potential (green and black *, respectively), as expected from the low-pass filtering properties of electrical synapses (e.g., Dugué et al., 2009). In invertebrates, gap junctions are formed by innexin molecules distinct from the connexins underlying vertebrate gap junctions (Phelan et al., 1998). To date no specific blockers are known. Since the vertebrate gap junction blocker carbenoxolone has been reported to block innexins in some cases (Sangaletti et al., 2014), we probed its effectiveness but found it unable to block the spike-triggered V_m transients in the LGMD (Supp. Fig. 2C). Hence, to further rule out IPSPs as the source of the transient hyperpolarizations, we applied the $GABA_A$ receptor blocker picrotoxin to dendritic field C and verified that they remained unaffected (Fig. 2G; n = 5 animals).

Next, we reasoned that IPSPs following spontaneous spikes of medullary DUB neurons might be difficult to resolve due to the relatively large noise of the spontaneous LGMD V_m (Fig. 2A). Hence, we stimulated the medullary neurons with small edges moving across the screen (see below for details) and computed spike-triggered averages of the simultaneously recorded LGMD V_m. Under these conditions, we could indeed observe a reliable IPSP generated in the LGMD by the DUB medullary neurons (Fig. 2H, *). This IPSP disappeared in randomized controls where averaging of the LGMD V_m was not coupled to the spikes of the studied cluster (Supp. Fig. 2C). Additionally, the IPSP was nearly abolished by puffing picrotoxin (~200 μM; Methods) on dendritic field C of the LGMD (Fig. 2H, PCTX). Interestingly, the transient hyperpolarization described above could be seen both before and after picrotoxin application further confirming that its origin is unrelated to $GABA_A$ receptor activation (Fig. 2H, arrowhead). We repeated this experiment in a total of six animals and computed the mean IPSP elicited by the visual stimulus presented at six locations on the screen before and after picrotoxin application.

As illustrated in Fig. 2I, the size of the visually evoked IPSP varied from animal to animal and from location to location (see below), but picrotoxin reliably reduced it in all animals. In five of the six experiments, one of the recorded units did not yield a spike-triggered membrane potential hyperpolarization in the LGMD, with an LGMD V_m spike-triggered average resembling that of the 3rd unit in Fig. 2D (orange trace). In those cases, we compared responses before and after picrotoxin application and could not find any indication of the presence of a spike-triggered IPSP during edge motion. Thus, units that did not exhibit the signature of an electrical synapse with the LGMD were also not chemically connected to it. To summarize this series of experiments, a subset of DUB-recorded medullary neurons provides synaptic input to the LGMD. This input arises both through an electrical and a chemical synapse. The electrical signature of the synaptic connection can be resolved from the spontaneous activity of DUB medullary neurons using spike-triggered averages of the LGMD V_m. In contrast, the inhibitory $GABA_A$ mediated IPSP cannot be resolved from spontaneous activity but is evident in visually evoked, spike-triggered and averaged activity. This spike-triggered visually-evoked IPSP is largely abolished by the $GABA_A$ blocker picrotoxin.

In total, we recorded from 3 to 4 medullary DUB neurons per animal across 150 animals. Of those over 60% were electrically connected to the LGMD. Across our data sample the spontaneous activity of these extracellularly isolated units was 17.5 ± 12.7 spks/s (mean, s.d.) and was not significantly different for neurons electrically connected to the LGMD (15.9 ± 6.7 spks/s; $p = 0.21$, rank-sum test). The peak amplitude of spike-triggered transient hyperpolarizations had a broad range (Supp. Fig. 2D). However, we found consistently across animals, that the unit having the largest extracellularly recorded spike always generated the largest spike-triggered transient hyperpolarization of the LGMD V_m (Supp. Fig 2E, mean amplitude: -0.11 mV, s.d.: -0.04 mV). Its median trough latency was also slightly longer than that of other medullary DUB neurons presynaptic to the LGMD (Supp. Fig. 2F).

Medullary DUB neurons presynaptic to the LGMD have wide spatial receptive fields.

Previous anatomical work suggested that OFF inhibitory inputs to dendritic field C of the LGMD may originate from neurons with receptive fields spanning about 8x12° (Rowell et al, 1977; Strausfeld and Naessel, 1981). To map the receptive fields of the medullary DUB neurons presynaptic to the LGMD, we used OFF edge visual stimuli translating with a constant speed at various locations in the visual field. More specifically and as illustrated in Fig. 3A (insets), the edges occupied ¼ of the height (18.8°) or width (22.8°) of the screen and translated at a speed of 28.6 °/s either along the dorso-ventral or along the antero-posterior axis, respectively. The instantaneous firing rate (IFR) of medullary DUB neurons often exhibited a transient burst immediately after the moving edge had entered the screen (Fig. 3A, arrows). After that, the IFR returned close to its spontaneous level (dashed lines in Fig. 3A) before tracking the stimulus as it crossed the screen. The strongest sustained responses were obtained for edges moving close to the center of the screen along the dorso-ventral axis, irrespective of the direction of motion, as illustrated in the top left panel of Fig. 3A. Responses along the antero-posterior axis were not as sustained (Fig. 3A, top right panel) while responses decreased as the stimuli moved

closer to the edges of the screen irrespective of motion direction (Fig. 3A, bottom panels). The spatial receptive field obtained by averaging and spatially smoothing the firing rate of medullary DUB neurons across 5 locusts with similar receptive fields is shown in Fig 3B. As may be seen from this figure, the receptive fields are considerably broader than expected.

We also mapped the spatial receptive fields of medullary DUB neurons presynaptic to the LGMD in 5 locusts using edges half as wide as those employed here. This yielded better spatial resolution at the expense of lower firing rates and thus increased noise. The results resemble those presented here and are illustrated in Supp. Fig. 3. Next, we computed the center of mass of the spatial receptive field and its moments about the azimuth and elevation axes in 16 medullary DUB neurons presynaptic to the LGMD (recorded in 10 locusts). As illustrated in Fig 3C, their receptive fields were equally broad as those illustrated in Fig. 3B, covering a large part of the central visual field.

Speed tuning of medullary DUB neurons presynaptic to the LGMD.

We then examined the dependence of the firing rate of medullary DUB neurons presynaptic to the LGMD on the speed of moving edges. We used 6 speeds varying from 7.1 to 227.2 °/s based on an earlier characterization of speed tuning in the LGMD (Krapp and Gabbiani, 2005). The width of the moving edge was ¼ of the width of the screen, like in the experiments described above. As illustrated in the top left panel of Fig. 4A, at a speed of 7.1 °/s the OFF-edge stimulus triggered a transient burst of firing (arrow) just after it entered the screen (left red vertical line). Soon thereafter, the firing rate returned to its spontaneous level and then ramped up as the stimulus entered the most sensitive part of the neuron's spatial receptive field. As the edge moved out of the receptive field, the neuron's firing rate gradually decreased back towards its spontaneous level. At intermediate speeds, the transient burst caused by the stimulus entering the screen was followed by a short period of silence (Fig. 4A, 28.4 º/s and 56.8 º/s). At the highest speeds, the transient burst merged with the spatial receptive field response (Fig. 4A, 272.2 º/s). The peak of the medullary DUB neurons' IFR in their receptive field increased logarithmically with speed. This is illustrated across five animals for motion along the dorso-ventral axis in the left plot of Fig. 4B and for antero-posterior motion in the right plot (dashed lines). In these plots, we pooled data obtained for both directions of motion (e.g., dorso-ventral and ventro-dorsal) as no significant difference could be discerned (see also below). This figure also reveals a weak dependence of speed tuning with the position of the moving edge along the dorso-ventral axis (left panel) and a more pronounced one along the antero-posterior axis (right panel), with higher responses at higher elevations.

The dashed lines in Fig. 4B represent log-linear fits of the peak firing rates as a function of speed at each stimulus location and show that a log-linear model faithfully describes the data. We also tested linear models of the peak firing rates as a function of speed, but in two of the stimulus locations along either the dorso-ventral or antero-posterior direction, log-linear plots fitted better than linear plots (e.g., Fig. 4B, left panel, black dashed line, $R^2 = 0.91 \pm 0.05$ for log-linear and $R^2 = 0.81 \pm 0.11$ for linear fit, $p = 0.0476$; blue dashed line, $R^2 = 0.92 \pm 0.03$ for log-linear and $R^2 = 0.79 \pm 0.08$ for linear fit, p =

0.0079, one-sided rank sum test). These results are similar to those reported for the dependence of the mean firing rate of the LGMD as a function of speed for localized moving stimuli (Krapp and Gabbiani, 2005). To confirm the lack of directional selectivity, we used edges moving in four directions at a location close to the center of the receptive field, as illustrated in Fig. 4C, to derive a polar plot of the responses. The polar plot is depicted in Fig. 4D. It shows that the firing rates in the four moving directions were nearly identical, and that they increased uniformly with speed. Similar results were obtained in 5 neurons. In summary, these results suggest no direction selectivity among the recorded medullary DUB neurons presynaptic to the LGMD, but a firing rate that is dependent on edge speed. Finally, we confirmed the dependence of the medullary DUB neurons' peak firing rate on the size of moving edges already noted in the context of Supp. Fig. 3 by plotting their responses as a function of edge size (Supp. Fig. 4).

The response to looming stimuli of medullary DUB neurons is tightly coupled to that of the LGMD.

As shown in Fig. 1, the firing rate of the LGMD in response to looming stimuli has a characteristic profile, gradually increasing, peaking and then decaying towards the time of collision. What is the corresponding response pattern of medullary DUB neurons presynaptic to the LGMD? The left panel of Fig. 5A illustrates the firing rate of two such medullary DUB neurons (cyan and green traces) recorded extracellularly simultaneously with the LGMD in response to a looming stimulus with $l/|v|$ = 20 ms. Both neurons demonstrated an activity profile resembling that of the LGMD (red traces in Fig. 5A). Their firing rate gradually increased, peaked and decayed towards the time of collision. Interestingly, the firing of the medullary DUB neurons outlasted that of the LGMD, a characteristic made clearer by pooling their activity (black traces in Fig. A). Similar results were observed at $l/|v|$ = 40 ms (Fig. 5A, middle panel) and at $l/|v|$ = 80 ms, although for this longer simulated approach the firing rate of the two medullary DUB neurons started to differ in their time courses in this example (Fig. 5A, right panel). In all cases, the medullary DUB neurons remained active for over 100 ms after the time of collision, before gradually regaining their spontaneous level.

Across our population sample, the spike counts of the LGMD and the medullary DUB neurons in response to looming stimuli were comparable (Fig. 5B). The timing of the medullary DUB neurons' peak firing rate, however, always followed that of the LGMD, as illustrated by population averages in Fig. 5C. Further, both medullary and LGMD peak times were tightly correlated with $l/|v|$ (Fig. 5C) and consequently with each other (ρ = 0.70 ± 0.21, n = 5). The difference in peak firing rate between medullary DUB neurons and the LGMD also increased with $l/|v|$ (Fig. 5D). These results suggest that the medullary DUB neurons presynaptic to the LGMD are well suited to contribute to the decay of the LGMD firing rate observed towards the end of a looming stimulus and are consistent with changes in firing rate observed in the LGMD after blocking feed-forward inhibition with picrotoxin (Gabbiani et al. 2005).

The example illustrated in Fig. 5A suggested that there might be some differences in the firing rate response to looming among units, particularly at $l/|v|$ = 80 ms. We thus carried out further data analysis to investigate whether any significant differences could be found between populations of medullary DUB neuron pairs recorded simultaneously. In seven such recordings, we labeled the neuron yielding the largest spike-triggered hyperpolarization in the LGMD as neuron 1, the other one being neuron 2 (c.f. Fig. 2B-D, green and blue clusters). Accordingly, these two neurons were labeled in green and blue in Fig. 5A. Across experiments, we found that the peak firing times to collision of both medullary units were significantly different among the three $l/|v|$ values studied. For neuron 1, the peak times to collision at $l/|v|$ = 20, 40, and 80 ms were -8.8 ± 26.9, 40.5 ± 12.4 and 108.0 ± 22.9 ms, respectively (mean ± s.d., n = 7; p = 0.0206 between $l/|v|$ = 20 and 40 ms; p = 0.0011 otherwise; one-sided rank sum test). The peak times to collision of unit two at $l/|v|$ = 20, 40, and 80 ms were -5.5 ± 8.9, 32.6 ± 16.8 and 131.2 ± 112.6 ms, respectively (p = 0.0011 for each paired comparison). However, no significant differences were found between the peak times to collision of the two units at each $l/|v|$ value. Additionally, there were no significant differences among the peak firing rates of both units at each $l/|v|$ value. Thus, the population of medullary DUB neurons presynaptic to the LGMD appears homogeneous with respect to its responses to looming stimuli.

The instantaneous firing rate of medullary DUB neurons is linearly related to the angular size of looming stimuli.

Next, we investigated which features of looming stimuli might be encoded by medullary DUB neurons presynaptic to the LGMD. From earlier work, we know that there are two variables closely associated with looming stimuli sufficient to describe the main characteristics of the LGMD's firing rate in response to a simulated object approach: angular size, $\theta(t)$, and angular speed, $\theta'(t)$ (Hatsopoulos et al. 1995; Gabbiani et al. 1999). Pre-synaptic excitatory inputs to the LGMD have been shown to encode the square of angular speed in their population response (Jones and Gabbiani, 2012); however, up to this point, no direct experimental evidence was available to evaluate the coding properties of inhibitory inputs to dendritic field C of the LGMD. Since, as shown above, medullary DUB neurons modulate their responses both to moving edge speed and size, and since these two variables are correlated during looming, a direct fit of responses to looming stimuli is needed to shed light on this issue. We thus plotted the pooled firing rates of medullary DUB neurons as a function of the angular size (Fig. 6A) and the angular speed (Fig. 6B) of looming stimuli. For all $l/|v|$ values, we used data starting 4 s before collision, when the stimulus is very small (< 2.3°; Fig. 5A), to the end of stimulus expansion. During faster looming stimuli ($l/|v|$ = 20 ms), the medullary IFR initially increased with the angular size and then saturated. However, with higher values of $l/|v|$, 40 or 80 ms, this saturation did not occur at larger angular sizes. The medullary DUB neurons' firing also increased in response to angular velocity at $l/|v|$ = 20 ms, but rapidly reached a peak and then saturated. Saturation was also evident at higher $l/|v|$ values of 40 and 80 ms. These results suggest that medullary DUB neurons might better encode angular size than speed.

To test this hypothesis, we fitted for each animal linear models depending on angular size, angular speed or both variables. We found that angular size models well-described the medullary firing ($R^2 = 0.76 \pm 0.06$) and for all animals performed better than linear models of angular speed ($R^2 = 0.56 \pm 0.05$, $p = 0.01$ rank-sum test). Fig 6C shows the firing rates and angular size model for one example animal. Results from other animals are shown in Supp. Fig. 5. Models using both size and speed provided only a slight improvement over size alone (mean $R^2 = 0.76$ vs 0.78, $p = 0.62$ rank-sum test). We also tested models of squared angular size and speed and log size and speed, but in all cases their performance was again less than that of angular size (squared size: $R^2 = 0.60 \pm 0.08$, $p = 0.01$; squared speed: $R^2 = 0.19 \pm 0.03$, $p = 0.0006$; log size: $R^2 = 0.42 \pm 0.11$, $p = 0.001$; log speed: $R^2 = 0.53 \pm 0.10$, $p = 0.004$; rank-sum tests). Additionally, a nonlinear, power law model of angular size did not significantly improve on the linear model (the adjusted R^2 increased by 0.01) with the best fit power being 1.05 ± 0.27 (mean ± s.d. across animals). As the peak firing rates differed between animals (Supp. Fig. 5), we normalized firing rates to each animal's peak rate to obtain a population model and thus test the consistency of the dependence of medullary DUB neurons' activity on angular size across animals. The resulting model (Fig. 6D) shows that the normalized medullary DUB neurons' firing rate exhibited a consistent increase with angular size at all tested $l/|v|$ values ($R^2 = 0.71$). Finally, the time course of medullary firing was estimated from the model shown in Fig. 6D for each of the tested $l/|v|$ values (Fig. 6E). In all cases the linear angular size model closely tracked the angular size of the stimulus ($R^2 = 0.79$, 0.93, and 0.90 for $l/|v| = 20$, 40, and 80 ms). These results support the notion that feed-forward inhibition mediated by medullary DUB neurons to the LGMD encodes the angular size of the looming stimulus.

Angular size is encoded by means of a small instantaneous firing rate population code

The large receptive field size of individual medullary DUB neurons means that single cells could encode relatively accurately the angular size of approaching objects. Additionally, the high degree of overlap of their receptive fields and similarity of responses means that there could be high redundancy in the information conveyed by these neurons to the LGMD. To characterize the population encoding of angular size by these medullary DUB neurons, we measured both the spontaneous and stimulus evoked spike correlations and tested the accuracy of angular encoding with different numbers of medullary units. For this analysis, each pair of simultaneously recorded units was analyzed independently for each trial, yielding 126 sample pairs from 97 stimulus trials (15 medullary neurons, 7 animals).

If the medullary DUB neurons presynaptic to the LGMD had non-overlapping receptive fields, one would expect negative correlations in their looming evoked responses, as the neurons would each be activated at different times during the stimulus. However, since their receptive fields are wide, with large overlap, positive spike correlations are predicted. Indeed, during looming stimuli, spike rate correlations averaged 0.28 with 106 of 126 pairs positively correlated ($p = 3.2 \cdot 10^{-16}$, signed-rank test; Fig. 7A, ordinate). To test whether these correlations were due to shared inputs, we also measured the spike rate

correlations of the same pairs during spontaneous activity. Surprisingly, this revealed fairly strong negative correlations of spontaneous activity for 80 of the 126 pairs ($p = 4.6 \cdot 10^{-4}$, signed-rank test; Fig. 7A, abscissa). This suggests that the stimulus evoked correlations are due to the overlapping receptive fields, but probably not to the statistics of their shared inputs.

Having firing rates weakly dependent on shared input statistics helps reduce the redundancy of the information these neurons convey to the LGMD. To test how many medullary DUB neurons are needed to encode angular size during looming, we treated each trial of each unit as independent (yielding sample population sizes of 13-45 pairs per animal from 7 animals; 126 total) and used bootstrap analysis to repeatedly sample different numbers of cells from the population and test their summed firing as a linear predictor of angular size (Fig. 7B). For each animal, a small number of units could reliably encode angular size (median of 5 cells to reach $R^2 \geq 0.8$). Sampling from more units improved performance to an average peak $R^2 = 0.91 \pm 0.04$ with less than 10 units needed to reach 95% of peak encoding for 6 out of 7 animals.

Discussion

Although feed-forward inhibition is omnipresent in neural circuits and known to play multiple roles related to the temporal processing of sensory information, little or no evidence relates its activation to the time-dependent coding of sensory stimulus variables. In this study, we have characterized the properties of presynaptic medullary DUB neurons providing inhibitory inputs to the LGMD in response to a variety of visual stimuli. We found that these neurons have wide receptive fields and a firing rate that depends on the size and speed of moving edges. In response to looming stimuli, the firing pattern of these neurons resembles that of the LGMD, gradually increasing and peaking before the time of collision. Over its rising phase, the firing rate of medullary DUB neurons is linearly related to the angular size of the looming stimulus, suggesting that they encode as a small, homogeneous population the angular size of approaching objects. The current results combined with earlier ones (Gabbiani et al., 2005) indicate that medullary DUB neurons play a critical role in terminating the excitation triggered in the LGMD by looming stimuli.

Identifying presynaptic LGMD neurons through spike-triggered averaging of the LGMD Vm.

By simultaneously recording extracellularly from the DUB and intracellularly from dendritic field C of the LGMD we identified medullary DUB neurons whose spikes elicited transient hyperpolarization and visually evoked IPSPs in the LGMD (Fig. 2). This is notable because other attempts we made to identify neurons presynaptic to the LGMD by this method failed. Initially, we hoped to characterize excitatory presynaptic neurons to the LGMD by inserting extracellular electrodes in the ventro-posterior part of the medulla, where excitatory presynaptic afferents should be preponderant, and an intracellular electrode in dendritic field A of the LGMD, which is easier to target than

field C. However, we were unable to find synaptically connected pairs through spike-triggered averaging, despite attempts in more than fifteen animals. This negative result may be due to the large number of medullary neurons contacting field A, generating substantial membrane noise, or to the recording electrode being placed too far from the distal dendritic tips where most inputs impinge, or to the fact that their synapses might not possess a highly reliable electrical component. Similarly, pilot experiments in several animals showed that spike-triggered changes in membrane potential could not be evidenced for medullary DUB neurons if the LGMD recording was made in dendritic field A. Presumably, this results from severe attenuation of V_m signals from dendritic field C to A, due to the extended electrotonic structure of the LGMD (Peron et al. 2007).

The timing of the spike-triggered hyperpolarization relative to medullary DUB neuron spikes was very short, on the order of 0.05-0.1 ms on average, with a spread of ~0.3 ms. This short interval is likely due to the time needed for the presynaptic spike to propagate from the recorded axon to the extracellular electrodes and to slight variations in the positioning of the extracellular electrodes relative to the recorded neurons. Although the vertebrate gap-junction blocker carbenoxolone was ineffective at blocking the spike-triggered hyperpolarization, other gap junction blockers or modulators could be tried in future experiments. Despite this, a preponderance of evidence points to a mixed electrical and chemical synapse between medullary DUB afferents and the LGMD. Similar mixed electrical/chemical synapses have been documented between the LGMD and the DCMD (Rind,1984; O'Shea and Rowell, 1975b; Killmann and Schürmann, 1985).

Mechanisms of DUB-mediated feed-forward inhibition in the LGMD

In our experiments, locally puffing GABA near dendritic field C significantly reduced the number of LGMD spikes elicited by looming stimuli. Conversely, puffing the $GABA_A$ blocker picrotoxin onto dendritic field C increased and prolonged responses to the same stimuli (Gabbiani et al. 2002, 2005). As we have shown, picrotoxin also abolished spike-triggered visual IPSPs from medullary DUB neurons. In earlier work, immuno-gold tagged GABA antibody staining showed the absence of GABA receptors on dendritic field A, suggesting that GABA-mediated inhibition is localized in dendritic fields B or C (Rind and Simmons, 1998). Our results show that electrical stimulation of the DUB induces IPSPs in the LGMD. Conversely, lesioning the DUB abolishes inhibition to OFF stimuli (Rowell et al. 1977). Thus, a large body of evidence suggests that feed-forward inhibition to dendritic field C of the LGMD is mediated by $GABA_A$ gated chloride channels activated through medullary DUB axons.

Wide receptive fields of presynaptic inhibitory neurons

Up to now, it was thought that the dorsal uncrossed bundle (DUB) conveyed its inhibitory inputs to dendritic field C through ~500 axons originating from cells with bodies in the proximal medulla (Elphick et al., 1996). Based on anatomical considerations, the receptive fields of these neurons were expected to cover ~8×12 º of the visual field (Rowell et al, 1977; Strausfeld and Naessel, 1981). Our results, however, do not support this hypothesis. The medullary DUB neurons presynaptic to the LGMD

that we characterized had wide receptive fields, at least on the order of ~40×40 º. Furthermore, only a small number of them was required to account for the angular size dependence of feed-forward inhibition over the course of a looming stimulus. Thus, it appears likely that the medullary DUB neurons presynaptic to the LGMD characterized here build a population much smaller in size than the ~500 neurons characterized in earlier work. We conclude that there must be at least two distinct populations of neurons within the DUB: the small-numbered population we studied electrophysiologically, and the larger-numbered population that was evidenced anatomically in earlier work.

Although we could record simultaneously only 2 or 3 medullary DUB neurons presynaptic to the LGMD, we have evidence to suggest that their sampling was not random across animals. For instance, and as illustrated in Supp. Fig. 2F, the neuron yielding the largest spikes in the extracellular recordings invariably yielded the largest spike-triggered membrane potential hyperpolarization in the LGMD. This suggests that either we were always recording from the same neuron across animals, and that this neuron has a larger axon than other ones having similar electrophysiological properties, or, alternatively, that there exists a small population of such neurons with tightly overlapping receptive fields. Based on our results, the role played by the 500 small receptive field neurons characterized anatomically remains to be determined. For instance, these neurons may not provide feed-forward inhibition as previously inferred from indirect anatomical and electrophysiological evidence. In *Drosophila*, the properties of two types of wide-field excitatory medullary neurons have been recently described: the Lawf2 neurons provide suppressive feedback to large monopolar cells in the lamina (Tuthill et al., 2014) and the Tm9 neurons play an important role in directional motion detection (Fisher, 2015). However, no wide-field inhibitory neurons have been described to the best of our knowledge, and neither have their coding characteristics been studied in the context of motion detection, either in *Drosophila* or in other preparations.

Medullary DUB neurons presynaptic to the LGMD encode angular size during looming.

The firing rate of the LGMD can be described by a multiplication of the angular speed of an approaching object ($\theta'(t)$) and a negative exponential of its angular size ($\exp(-\alpha\theta(t))$) through a logarithmic-exponential transformation,

$$f(t) \propto \exp\left[\log\left(\theta(t)\right) - \alpha\theta(t)\right]$$

(Hatsopoulos et al. 1995; Gabbiani et al. 1999; Gabbiani et al., 2002). This formula suggested that the second, inhibitory term could arise from angular-size dependent inhibition provided by medullary DUB neurons. The current experiments confirm this hypothesis. Notably, in previous simulations we had predicted that the population response of medullary DUB neurons would encode the squared angular size, $\theta(t)^2$, instead of $\theta(t)$ (Jones and Gabbiani, 2012). In that work, we had assumed that feed-forward inhibition is mediated by a large population of independent inhibitory neurons with small receptive fields, based on the assumption that they corresponded to the population of DUB neurons characterized anatomically. Under these assumptions, each neuron transmits information about local luminance changes over the area of its receptive field and thus at the population level over the angular area covered by the stimulus, which

is proportional to $\theta(t)^2$. In contrast, the current results show that the size-dependent signals originating from individual ommatidia are pooled by a few medullary DUB neurons at most before reaching the LGMD, leading to a significant compression and an instantaneous firing rate code proportional to $\theta(t)$. Based on these results, inhibitory input to the biophysical model of Jones and Gabbiani (2012) needs (at a minimum) to be revised to account for this difference. The encoding of angular size by medullary DUB neurons and the tight correlation between their peak firing rate and that of the LGMD agrees well with results showing that block of feed-forward inhibition plays a central role in terminating the LGMD response to looming stimuli (Gabbiani et al., 2005). Since the decay of the LGMD's firing rate following its peak plays an important role in triggering escape behaviors to looming stimuli (Fotowat et al., 2011; Fotowat and Gabbiani, 2011), we conclude that the encoding of angular size by feed-forward inhibition does as well.

In other systems, looming-sensitive neurons with response properties resembling those of the LGMD have been described (e.g., Wu et al, 2005; Sun and Frost 1998; Preuss et al. 2006; de Vries and Clandinin 2012; Olivia and Tomsic 2014; Dunn et al. 2016; Fotowat and Gabbiani, 2011; Liu et al, 2011), but little is known about how inhibitory neurons code for the parameters of an approaching stimulus. Interestingly, in *Drosophila* recent results have evidenced the existence of an angular size-dependent inhibitory input to the giant fiber, a neuron also involved in visually guided collision avoidance behaviors (von Reyn et al., 2017). However, the neuron or neurons mediating this inhibition remain to be identified and characterized electrophysiologically. It is thus possible that in this system and in others were feed-forward inhibition plays a role in timing neural responses to sensory stimuli, the inhibitory neurons mediating feed-forward inhibition also carry detailed time-varying sensory stimulus information. This would confer to feed-forward inhibition a role on par with that of feed-forward excitation in shaping neural computations.

Experimental Materials and Methods

Animals. Eight to ten week-old adult locusts (*Schistocerca americana*) of both sexes were used for experiments. The locusts were maintained under a 12:12 h light:dark life cycle at a mean temperature of 31°C and fed with wheat seedlings and oat meal. The dissection was carried out as described previously (Gabbiani et al., 2002). Briefly, the legs, wings and antennas of locusts were removed. The locust body was mounted in a plastic holder with the dorsal side facing upward. The head capsule was opened and the muscles above the optic lobes and brain were removed. The air sacs above the ventral nerve cords were removed to expose them. During the dissection, the whole head was immersed in ice-cold locust saline solution. The right eye was fixed with bee wax to the holder. The entire procedure lasted approximately 1.5 h. During experiments, the head remained immersed in saline, except for the right eye which was exposed to the stimulus-displaying monitor.

Electrophysiology. Thin-walled borosilicate glass capillaries (1.2/0.9 mm outer/inner diameter; WPI, Sarasota, FL) were used for making intracellular electrodes to record from the LGMD. A Sutter P-97 Flaming/Brown type micropipette puller (Novato, CA) was used to fabricate sharp electrodes which were filled with an internal solution containing 1.5 M KAc, 1M KCl and 10 mM Alexa 594 (final micropipette resistance: 8 – 20 MΩ). Bath solutions included 140 mM NaCl, 5 mM KCl, 5 mM $MgCl_2$, 5 mM $CaCl_2$, 6.3 mM HEPES, and 4 mM $NaHCO_3$, and 73 mM Sucrose. The pH was adjusted to 7.0. All the intracellular recordings were recorded in bridge mode using a NPI amplifier (NPI electronics, Tamm, Germany). The electrode resistance and capacitance were compensated before approaching the surface of the optic lobe. The LGMD and the descending contralateral movement detector (DCMD) have a 1:1 spiking correspondence (O'Shea and Williams, 1974). The LGMD was thus identified using DCMD spikes recorded extracellularly from the ventral nerve cord with a pair of stainless steel hook electrodes. The spikes of the DCMD were the biggest ones recorded extracellularly, and could therefore easily be identified. The LGMD was initially stained with Alexa 594 by iontophoresis (- 2 nA current pulses, alternating between on and off every second). Next, the sharp electrode was inserted into the thin dendrites of dendritic field C receiving feed-forward inhibitory inputs under visual control. Initially, sharp tungsten electrodes with an input impedance of 0.5 and 5 MΩ (FHC, Bowdoin, ME) were compared to record spikes from the medulla. Use of the lower impedance tungsten electrode resulted in a better yield, with a larger number of isolated units. Therefore in the following experiments we always used a pair of sharp tungsten electrodes with an input impedance of 0.5 MΩ. They were positioned in the DUB at the level of the proximal medulla, near the inhibitory branches of the LGMD to record the extracellular spikes generated by medullary DUB neurons. The distance between the paired tungsten electrodes amounted to 50-75 μm and their distance to the intracellular electrode positioned in dendritic field C of the LGMD was at least 200 μm. Earlier paired recordings in the optic lobe have shown that extracellular spikes can be recorded up to 100 μm away from a neuron impaled using an intracellular electrode, with no noticeable interference between the recordings (Wehr et al. 1999). The location of the DUB was identified by electrical stimulation with an amplitude and duration varied from 15 to 320 μA and from 0.1 to 1 ms through the sharp

669 tungsten electrodes using a stimulus isolator (DS3, Digitimer Ltd., Fort Lauderdale, FL)
670 which produced characteristic IPSPs in the LGMD (Fig. 1F). The extracellularly recorded
671 DCMD and medullary spikes were amplified through a differential AC amplifier (A-M
672 Systems 1700; Sequim, WA) and an instrument amplifier (Brownlee 440; NeuroPhase,
673 Santa Clara, CA). All the recordings were sampled at 19927.5 Hz. A chlorided silver wire
674 was placed in the bath solution and used as a reference electrode.
675
676 ***Visual stimulation.*** Looming stimuli and moving edge stimuli were generated using
677 custom software with a computer running the QNX4 real-time operating system (QNX,
678 Ottawa, ON) and displayed through a cathode ray tube monitor with a 200 Hz refresh
679 rate. The right eye was positioned to face the center of the monitor from a distance of 20
680 cm. In these experiments, looming stimuli refer to black disks on a white screen
681 expanding rapidly in size from a tiny point at the center of the screen, simulating the
682 approach of an object with a half-size l and a constant translation speed v (Gabbiani et al.,
683 1999, 2005). The time course of approach is characterized by the ratio $l/|v|$. Three $l/|v|$
684 ratios were used, $l/|v|$ = 20, 40 and 80 ms. Looming stimuli were presented every other 4
685 minutes. Moving edge stimuli were used to map the receptive field of the medullary DUB
686 neurons. In these experiments, a black edge on a white screen moved either from
687 posterior to anterior or from ventral to dorsal, and vice versa, with a constant speed. The
688 width of the edge was one–eighth or one-fourth of the screen dimension perpendicular to
689 the edge movement direction. Thus, when the edge moved dorso-ventrally its width was
690 18.7°; when the edge moved antero-posteriorly, its width was 22.7°. The edge speed took
691 the following six values: 7.1, 14.2, 28.4, 56.8, 113.6, and 227.2 °/s to measure the
692 relationship between speed and the medullary DUB neurons' firing rate. A speed of
693 28.4 °/s was used to map the spatial receptive fields, with additional experiments at
694 14.3 °/s. Edge stimuli were presented at an interval of 5 s and were cycled through all
695 positions and motion directions in turn to minimize potential habituation of the medullary
696 neurons' firing rate.
697
698 ***Injection of picrotoxin and GABA in the lobula.*** To study the pharmacological
699 properties of feed-forward inhibition, picrotoxin (5 mM) and GABA (10 mM) dissolved
700 in water were puffed along the dorsal edge in the lobula, close to the region where the
701 inhibitory dendrites of LGMD's field C arborize. The injected solution contained 0.5 %
702 of the colorant fast green to visualize the tip of the injection pipette and the amount of
703 solution injected in the lobula. The injection pipette tip diameter varied between 1 and 2.5
704 µm. After injection, the dye diffused around the injection site and stayed confined to the
705 lobula. A picospritzer was used to control the duration and the puffing pressure (8 psi/55
706 kPa; WPI, Sarasota, FL). Based on earlier work (Dewell and Gabbiani, 2017), the
707 estimated final concentration of drugs at the level of field C was ≤ 200 µM (picrotoxin)
708 and ≤ 300 µM (GABA).
709
710 ***Data analysis and statistics.*** Custom Matlab code was used for data analysis. The
711 medullary DUB neuronal spikes were sorted following general principles exposed in
712 Pouzat (2016), using a spike-sorting program modified from publicly available code
713 described in Pouzat and Detorakis (2014). Briefly, the data were first normalized, before
714 detecting spikes with a threshold and building an event dictionary consisting of non-

overlapping spike waveforms. After performing principal component analysis to reduce dimensionality, the data set was visualized using the grand tour visualization technique implemented in the software GGobi. Typically, individual spike clouds were well separated and could be clustered using K-means classification based on the visualization step. Next, the delay of individual spike events relative to the spike template for a given cluster was estimated and cancelled, before subtracting from the original recording each event identified as being from that cluster. This last step of the procedure (called 'peeling' in Pouzat and Detorakis, 2014) was repeated until no further spikes could be identified in the original recording. To calculate instantaneous firing rates (IFRs) during looming stimuli, the spike trains of the LGMD and the medullary DUB neurons were convolved with a Gaussian filter having a standard deviation of 20 ms. The medullary neurons' IFR evoked by edge movement was calculated as briefly explained below (see Gabbiani and Krapp, 2006 for details). For each spike train, the firing rate before the time of the first spike was set to 0 ($f(t) = 0$ if $t<t_1$, where 1 is the index of the first spike); the firing rate at the time of the first spike was calculated as half the inverse of the time interval between the first and second spike ($f(t) = 0.5/(t_2-t_1)$ if $t = t_1$); then, the firing rate at a time between two neighboring spikes was calculated as the inverse of the corresponding inter-spike interval (ISI, $f(t) = 1/(t_i-t_{i-1})$ if $t_{i-1}<t<t_i$); the firing rate at the time of subsequent spikes was calculated as the average of the inverse inter-spike intervals immediately preceding and following it ($f(t) = 0.5/(t_i-t_{i-1}) + 0.5/(t_{i+1}-t_i)$ if $t = t_i$); the firing rate at the time of the last spike was half of the inverse of the last ISI ($f(t) = 0.5/(t_n-t_{n-1})$ if $t = t_n$, where n is the index of the last spike); the firing rate after the time of the last spike was set to 0 ($f(t) = 0$ if $t>t_n$). Above, t_1 and t_n refer to the first and last spike time, $f(t)$ is the IFR at a certain time t, and i indexes the spikes.

The membrane hyperpolarization evoked by electrical stimulation was calculated as the difference between the LGMD mean V_m within 0.1 s before the artifact caused by the electrical stimulus and the minimum V_m within 0.02 s after the electrical stimulus artifact. Because electrical stimulation always elicited initially excitation in the LGMD we could only estimate an upper bound in the onset latency of inhibition. This latency of inhibition, which we call the earliest detectable latency, was calculated as the time difference from the time of the electrical stimulation artifact to the subsequent time when LGMD V_m returned to the mean V_m value computed within 0.1 s before the artifact, as explained above.

The Wilcoxon signed-rank test was used to compare the statistical differences between groups treated with or without picrotoxin or GABA. Unless denoted with mean ± s.e. (standard error), all the data were described as mean ± s.d. (standard deviation).

For linear modeling of the data presented in Fig. 6 and the corresponding text, we used the Matlab function 'fitlm' which generates a best fit from a least-squares linear regression. Simple linear models with constant and linear terms (no interaction terms) were employed using the summed firing rates of the medullary neurons. The peak firing rate of individual medullary neurons and the number of neurons recorded both varied across animals. So, before we averaged data from multiple animals (Fig. 6D, E), the firing rates for each animal were normalized to the peak firing rate of that animal. The

quality of the fit for each model was measured by the adjusted-R^2 statistic and the F-statistic of the model's linear component. For comparisons between models (e.g., comparing the $\theta(t)$ model to $\theta'(t)$ model) a Wilcoxon rank-sum (Mann-Whitney U) test was used to compare the ajusted-R^2 values of the corresponding models for each animal.

Analyses of spike correlations (Fig. 7) were conducted among pairs of units recorded in the same stimulus trial. If 5 stimulus trials were presented to an animal in which 3 medullary units were recorded, this yielded 15 sample pairs (5 comparisons between units 1 and 2, 5 between units 1 and 3, and 5 between units 2 and 3). In total 126 paired comparisons were made from 15 medullary units recorded from 7 animals. For the spontaneous correlations, the firing of each sample pair just before the start of the visual stimulus was analyzed (2.1 ± 1.0 s of recording with average spontaneous firing rates of 24 ± 13 spk/s). The data were down-sampled to 200 Hz and instantaneous firing rates were calculated with Gaussian convolution as described above.

To determine how many medullary DUB neurons were needed to accurately predict the stimulus angular size, we binned the data and used a bootstrap sampling method. The time periods corresponding to 1° increments of the stimulus angular size were determined for each stimulus trial (in total 209 trials from 7 animals) and the average IFR of individual medullary units was measured within each corresponding time period. This was done to facilitate combining responses to stimuli with different $l/|v|$ values. Once the data was binned according to the stimulus angle that evoked it for each trial, 1000 bootstrap samples (using Matlab 'bootstrap' function) were taken with different numbers of cells ranging from 1 to the population size for that animal. For each of the 1000 draws for each sample size, the firing rates of the drawn units were summed together and fit to the stimulus size. The average quality of those fits (R^2) is displayed in Fig. 7B.

Figure Legends

Figure 1. Feed-forward inputs from the dorsal uncrossed bundle (DUB) to field C of the LGMD are inhibitory. (**A**) Alexa 594 stain of the LGMD illustrating its three dendritic fields, labeled A, B and C. (**B**) NADPH-diaphorase staining of the locust optic lobe revealing the dorsal uncrossed bundle (DUB) terminating in the anterior lobula. Abbreviations: La., lamina; 1st O. Ch., first optic chiasm; e. Me., external medulla; Lo., lobula. Adapted from Elphick et al. (1996). (**C**) Close-up view of the recording configuration. The optic lobe, delineated by the white dashed lines, lies beneath the locust right eye (left). Brown and yellow lines represent the location of the extracellular electrodes and the intracellular one positioned in field C of the LGMD, respectively. The LGMD was stained with Alexa 594 and its three dendritic fields can be seen in this low magnification micrograph (arrowheads labeled A, B and C). (**D**) Intracellular recording from LGMD's field C (middle, control) in response to a looming stimulus ($l/|v|$ = 40 ms, top). After puffing GABA on dendritic field C (bottom, GABA), the number of spikes was substantially reduced. 0 is the resting membrane potential. Top inset: schematic of the stimulus configuration. θ: half-angle subtended at the retina, l: stimulus half-size, v: approach speed. (**E**) mean instantaneous firing rate of the LGMD before and after GABA puffing. Shaded regions denote ±1 s.d. (n = 5 animals). Inset: the mean firing rate averaged over the entire trial was significantly smaller after GABA application ($p = 0.03$, n = 5, Wilcoxon signed-rank test). For each box plot, the red line shows the median, the upper and lower box limits bracket 75% of the distribution, and the "whiskers" above and below each box show the locations of the minimum and maximum. (**F**) Electrical stimulation through the extracellular electrodes, (C), during a looming stimulus with $l/|v|$ = 40 ms (top) triggered a compound IPSP (bottom, arrow) in the LGMD. Red line indicates the time of electrical stimulation.

Figure 2. Medullary spike-triggered hyperpolarizations and IPSPs in field C of the LGMD. (**A**) Example traces of spontaneous multiunit activity of medullary neurons recorded from the DUB (top) and the LGMD's membrane potential recorded simultaneously (bottom). Inset: close-up view of LGMD V_m. (**B**) The spikes of medullary neurons were sorted into 3 clusters using PCA and K-means classification. (**C**) Spike waveforms corresponding to the clusters in (B). The solid and dashed lines correspond to signals recorded at electrode 1 and 2, respectively. (**D**) Medullary neuronal spikes from clusters 1 and 2 triggered rapid hyperpolarizations of the LGMD V_m in field C, usually preceded by a smaller transient depolarization (green and orange arrowheads). The * symbols indicate the through of the hyperpolarization. Gray arrowhead: post-hyperpolarization rebound. Dashed lines show the mean ± 4 s.d. of the membrane potential recorded before the medullary spikes. The 3rd cluster spikes (orange, bottom) do not affect the LGMD's V_m. (**E**) The time to the trough of the spike-triggered hyperpolarization for all the clusters with a significant through (> 4 s.d. of the mean membrane potential) relative to the time of extracellular medullary spike peak (n = 101 locusts). (**F**) Left, single spike-triggered hyperpolarization (green) superposed onto the simultaneously recorded extracellular spike triggering it (black). The dashed black line is the same extracellular spike shifted by 0.45 ms. Right, same for the mean spike-triggered hyperpolarization and the mean extracellular spike. (**G**) Application of picrotoxin

(PCTX) onto LGMD's dendritic field C does not abolish the spike-triggered hyperpolarization. (**H**) Spike-triggered visually evoked IPSP (*) is abolished by picrotoxin. Arrowhead indicates the spike-triggered hyperpolarization. (**I**) Reduction of mean spike-triggered visually evoked IPSPs following application of picrotoxin in six animals. The IPSPs were averaged from 5 to 50 ms after medullary spike time peak. Each pair of points represents a different stimulation location on the screen. (p-values from Wilcoxon signed-rank test).

Figure 3. Inhibitory medullary neurons presynaptic to the LGMD have wide receptive fields. (**A**) Instantaneous firing rate (IFR) responses of medullary neurons to OFF edges translating across the visual field. Left, response of one neuron to 18.8 º-wide edge motion (28.6 º/s) from dorsal to ventral (black) and from ventral to dorsal (red) centered at two azimuth locations. Right, response of a different neuron to 22.8 º-wide edge motion (28.6 º/s) from anterior to posterior (black) and from posterior to anterior (red) at two elevations. Insets indicate the direction of motion with arrowheads and the location of the edge on the screen. Point with coordinates (0,0) in elevation and azimuth, respectively, is eye center. Arrows indicate the brief spike burst elicited by the edge appearance on the screen. (**B**) Spatial receptive field obtained by computing the mean firing rate (after subtraction of the spontaneous activity) over five medullary DUB neurons to the stimuli illustrated in (A). Spatial smoothing was achieved by applying a 3×4º mean filter. (**C**) Location of the mean response (black and grey dots) and ±1 standard deviation along azimuth and elevation for 16 inhibitory medullary neurons presynaptic to the LGMD. Black dots indicate cluster with largest spike-triggered hyperpolarization in the LGMD and grey dots other clusters.

Figure 4. The instantaneous firing rate of medullary neurons presynaptic to the LGMD depends on OFF edge speed and is independent of movement direction. (**A**) Example instantaneous firing rates (IFRs) of one medullary neuron in response to an edge moving from dorsal to ventral with different speeds (7.1, 28.4, 56.8, and 227.2 º/s) at the second azimuth position on the screen (central inset). Top insets in each panel illustrate edge position on the screen. Red vertical lines indicated start and end time of motion. Blue curves are smoothed firing rates. Arrow in top panel illustrates the brief spike burst caused by the appearance of the stimulus on the screen. (**B**) Peak firing rates of medullary neurons for edges translating from dorsal to ventral and vice versa (left) at four locations on the screen (inset and arrowheads). Right, same as left for anterior to posterior motion and vice-versa (mean ± s.e.m.; n = 5 locusts). Intercepts and slopes from black to red, left: -5.37, -4.65, -4.44, -2.91 spk/s and 6.0, 5.52, 5.42, 4.38 spk/º; right: -6.39, -4.91, -5.22, -2.16 spk/s and 5.73, 6.79, 5.14, 2.77 spk/º. (**C**) Instantaneous firing rate (black) and filtered IFR (blue) of a medullary neuron for four edge motion directions and a speed of 28.4 º/s. (**D**) The averaged peak firing rates of medullary neurons across 5 locusts to OFF-edge motion in four different directions. Colors represent different speeds.

Figure 5. Responses of medullary DUB neurons presynaptic to the LGMD and of the LGMD to looming stimuli. (**A**) From left to right: example responses to looming stimuli at $l/|v|$ = 20, 40 and 80 ms (corresponding to three object approach velocities for a fixed object size). Top, the object angular size is plotted as a function of time to collision (t =

0) as the simulated object approaches towards the eye. Middle, instantaneous firing rate of medullary (Med) neurons (green and blue are individual neurons, black is summed across both units) and the LGMD (red) to looming stimuli. Bottom spike rasters indicating the spike times for five trials. Inset shows a schematic of the looming stimuli. (**B**) Spike count elicited by looming stimuli at the same three $l/|v|$ values (LGMD: mean ± s.d., n = 7 animals; Med: mean ± s.d., n = 15 neurons in 7 animals). (**C** and **D**) The time at peak firing rate relative to collision and the maximum firing rate for the same three $l/|v|$ values (mean ± s.d., n = 7 locusts). For medullary DUB neurons, values are reported for summed activity (black lines in A). Dotted lines represent linear fits.

Figure 6. The instantaneous firing rate of medullary DUB neurons presynaptic to the LGMD encodes the angular size of looming stimuli. (**A**) The instantaneous firing rate of medullary neurons increased as the angular size of looming stimuli increased (mean ± s.d., n = 7 locusts; firing rate summed over medullary DUB neurons, see Fig. 5A, and averaged across animals). Each panel shows a different $l/|v|$ value, $l/|v|$ = 20 (left), 40 (middle), 80 ms (right). During looming stimuli with the smallest $l/|v|$ value (faster velocity for a fixed object size) the firing rate saturated, but not during looming stimuli with larger $l/|v|$ values (slower velocities). (**B**) The instantaneous firing rate of medullary DUB neurons initially increased with angular velocity during looming stimuli. At higher angular speeds firing rates saturated. Note the decreased range of angular speeds for higher $l/|v|$ values (slower looming stimuli; mean ± s.d., n = 7 locusts). (**C**) Firing rate as a function of angular size for three $l/|v|$ values (colored lines) and linear fit (black line $R^2 = 0.85$, $p < 1 \cdot 10^{-9}$, F-test) in one example animal (data from other animals in Supp. Fig. 6). (**D**) After normalizing firing rates to each animal's peak firing rate, the linear model was fit to the population average (mean ± s.e., n = 6; $R^2 = 0.71$, $p < 1 \cdot 10^{-9}$, F-test). Colors as in (C). (**E**) Average response during looming approach (black lines and gray shadings are mean ± s.d., n = 6 locusts) with overlaid predicted responses from the linear model in (D) (red lines). For all three $l/|v|$ values the linear model predicts the time course of the medullary firing (R^2 = 0.79, 0.93, and 0.90 for $l/|v|$ = 20, 40 and 80 ms respectively).

Figure 7. A small population of medullary DUB neurons is sufficient to convey the angular size of looming stimuli. (**A**) Spike rate correlations between pairs of medullary neurons reveal slightly negative, significant average correlations of spontaneous activity (-0.07 ± 0.22, mean ± s.d., with 80 of 126 pairs negatively correlated, $p = 4.6 \cdot 10^{-4}$ signed-rank test). During looming stimuli, firing rate correlations increased to 0.28 ± 0.27, mean ± s.d., with 106 of 126 pairs positively correlated ($p = 3.2 \cdot 10^{-16}$, signed-rank test). Bars are histograms along each axis, with mean correlation values indicated by red dashed lines. (**B**) Bootstrap estimates of the number of medullary neurons needed to decode angular size. For each animal (blue lines) angular size could be estimated accurately with a small number of neurons, 5.3 ± 3.3 (mean ± s.e.) to reach an $R^2 \geq 0.8$. Black lines and gray shaded region show the mean ± 1 s.d. of the 7 animals.

Acknowledgements

We thank Dr. Holger and Dr. Jiang for comments on the manuscript. The work was supported by grants from the National Science Foundation (DMS-1120952), the National Institutes of Health (NIH) (MH-065339) and NEI Core Grant for Vision Research (EY-002520-37).

Author Contributions

H.W., R.B.D. and F.G. conceived the experiments; H.W. performed electrophysiology experiments; H.W., R.B.D. and Y.Z. analyzed data; H.W., R.B.D. and F.G. prepared figures and wrote the paper.

References

Blitz, D. M., and Regehr, W. G. (2005). Timing and specificity of feed-forward inhibition within the lgn. Neuron. *45*, 917-928.

de Vries, S.E.J., and Clandinin, T.R. (2012). Loom-Sensitive Neurons Link Computation to Action in the Drosophila Visual System. Curr Biol *22*:353–362

Dugué, G.P., Brunel, N., Hakim, V., Schwartz, E., Chat, M., Lévesque, M. Courtemanche, R., Léna, C., and Dieudonné, S. (2009). Electrical coupling mediates tunable low-frequency oscillations and resonance in the cerebellar Golgi cell network. Neuron *61*, 126-139.

Dunn, T.W., Gebhardt, C., Naumann, E.A., Riegler, C., Ahrens, M.B., Engert, F., and Del Bene, F. (2016). Neural Circuits Underlying Visually Evoked Escapes in Larval Zebrafish. Neuron *89*:613–628

Elphick, M.R., Williams, L., and O'Shea, M. (1996). New features of the locust optic lobe: evidence of a role for nitric oxide in insect vision. J. Exp. Biol, *199*, 2395-2407.

Fino, E., and Yuste, R. (2011). Dense inhibitory connectivity in neocortex. Neuron *69*, 1188-1203.

Fisher, Y.E., Leong, J.C., Sporar, K., Ketkar, M.D., Gohl, D.M., Clandinin, T.R., and Silies, M. (2015). A class of visual neurons with wide-field properties is required for local motion detection. Curr. Biol. *25*, 3178-3189.

Fotowat, H., and Gabbiani, F. (2011). Collision detection as a model for sensory-motor integration. Ann. Rev. Neurosci. *34*, 1-19.

Fotowat, H., Harrison, R.R., and Gabbiani, F. (2011). Multiplexing of motor information in the discharge of a collision detecting neuron during escape behaviors. Neuron. *692*, 147- 168.

Gabbiani, F., Cohen, I., and Laurent, G. (2005). Time-dependent activation of feed-forward inhibition in a looming-sensitive neuron. J Neurophysiol. *94*, 2150 -2161.

Gabbiani, F., and Krapp, H.G. (2006). Spike-frequency adaptation and intrinsic properties of an identified, looming-sensitive neuron. J. Neurophysiol. *96*, 2951–62

Gabbiani, F., Krapp, H.G., Koch, C., and Laurent, G. (2002). Multiplicative computation in a visual neuron sensitive to looming. Nature. *420*, 320-324.

Gabbiani, F., Krapp, H.G., and Laurent, G. (1999), Computation of object approach by a wide-field, motion-sensitive neuron. J Neurosci. *19*, 1122-1141.

Gabernet, L., Jadhav, S.P., Feldman, D.E., Carandini, M., and Scanziani, M. (2005). Somatosensory integration controlled by dynamic thalamocortical feed-forward inhibition, Neuron. *48*, 315-327.

Hatsopoulos, N., Gabbiani, F., and Laurent, G. (1995). Elementary computation of object approach by wide-field visual neuron. Science. *270*, 1000 -1003.

Homberg, U., and Würden, S. (1997). Movement-sensitive, polarization-sensitive, and light-sensitive neurons of the medulla and accessory medulla of the locust, *Schistocerca gregaria*. J. Comp. Neurol. *386*, 329-346.

Hu, B., Li, X., Zhou, Y., and Shou T. (2000). Effects of bicuculline on direction-sensitive relay cells in the dorsal lateral geniculate nucleus (LGNd) of cat. Brain Res. *885*, 87-93.

Isaacson, J.S., Solís, J.M., and Nicoll, R.A. (1993). Local and diffuse synaptic actions of GABA in the hippocampus. Neuron. *10*,165-175.

James, A. C., and Osorio, D. (1996). Characterisation of columnar neurons and visual signal processing in the medulla of the locust optic lobe by system identification techniques. J. Comp. Physiol. *A178*, 183-199.

Jones, P.W., and Gabbiani, F. (2012). Logarithmic compression of sensory signals within the dendritic tree of a collision-sensitive neuron. J Neurosci *32*, 4923-4934.

Kapfer, C., Glickfeld, L.L., Atallah, B.V., and Scanziani, M. (2007). Supralinear increase of recurrent inhibition during sparse activity in the somatosensory cortex. Nat. Neurosci. *10*, 743-753.

Killmann, F., and Schürman, F.W. (1985). Both electrical and chemical transmission between the 'lobula giant movement detector' and the 'descending contralateral movement detector' neurons of locusts are supported by electron microscopy. J. Neurocytol. *14*, 637-652.

Krapp, H.G., Gabbiani, F. (2005). Spatial distribution of inputs and local receptive field properties of a wide-field, looming sensitive neuron. J. Neurophysiol. *93*, 2240–2253.

Liu, Y.J., Wang, Q., and Li, B. (2011). Neuronal responses to looming objects in the superior colliculus of the cat. Brain. Behav. Evol. *77*, 193-205.

Mittmann, W., Koch, U., and Häusser, M. (2005). Feed-forward inhibition shapes the spike output of cerebellar Purkinje cells. J. Physiol. *563*, 369-378.

Norton, T.T., Holdefer, R.N., and Godwin, D.W. (1989). Effects of bicuculline on receptive field center sensitivity of relay cells in the lateral geniculate nucleus. Brain Res. *488*, 348-352.

Oliva, D., and Tomsic, D. (2014), Computation of object approach by a system of visual motion-sensitive neurons in the crab Neohelice. J Neurophysiol *112*:1477–1490

O'Shea, M., and Rowell, C.H.F. (1975a). Protection from habituation by lateral inhibition. Nature. *254*, 53-55.

O'Shea, M., and Rowell, C.H.F. (1975b). A spike-transmitting electrical synapse between visual interneurones in the locust movement detector system J. Comp. Physiol. *97*, 143-158.

O'Shea, M., and Williams, J.L.D. (1974). The anatomy and output connection of a locust visual interneurone; the Lobular Giant Movement Detector (LGMD) neurone. J. Comp. Physiol. *91*, 257-266.

Osorio, D. (1991). Mechanisms of early visual processing in the medulla of the locust optic lobe: how self-inhibition, spatial pooling and signal rectification contribute to the properties of transient cells. Visual. Neurosci. *7*, 345-355.

Ozeki, H., Finn, I. M., Schaffer, E. S., Miller, K. D., and Ferster, D. (2009). Inhibitory Stabilization of the Cortical Network Underlies Visual Surround Suppression. Neuron. *62(4)*, 578-592.

Perez-Orive, J., Mazor, O., Turner, G.C., Cassenaer, S., Wilson, R.I., and Laurent, G. (2002). Oscillations and sparsening of odor representations in the mush-room body. Science. *297*, 359-365.

Perisse, E., Owald, D., Barnstedt, O., Talbot, C.B., Huetteroth, W., and Waddell, S. (2016). Aversive Learning and appetitive motivation toggle feed-forward inhibition in the Drosophila mushroom body. Neuron. *90*, 1086-1099.

Peron, S.P., and Gabbiani, F. (2009). Spike frequency adaptation mediates looming stimulus selectivity in a collision-detecting neuron. Nat. Neurosci. *12*, 318-326.

Peron, S.P., Krapp, H.G., and Gabbiani, F. (2007). Influence of electrotonic structure and synaptic mapping on the receptive field properties of a collision-detecting neuron. J Neurophysiol. *97*:159–177.

Phelan, P., Bacon, J.P., Davies, J.A., Stebbings, L.A., Todman, M.G., Avery, L., Baines, R.A., Barnes, T.M., Ford, C., Hekimi, S., Lee, R., Shaw, J.E., Starich, T.A., Curtin, K.D., Sun, Y.A., and Wyman, R.J. (1998). Innexins: a family of invertebrate gap-junction proteins. Trends Genet. *14*, 348-*349.*

Pouille, F., and Scanziani, M. (2001). Enforcement of temporal fidelity in pyramidal cells by somatic feed-forward inhibition. Science. *293*, 1159-1163.

Pouzat, C. (2016). Analysis of Extracellular Recordings. In: Brain-Computer Interfaces 1: Methods and Perspectives, edited by M. Clerc, L. Bougrain and F. Lotte, Wiley & Sons: Hoboken, NJ.

Pouzat, C., and Dektorakis G.I. (2014). SPySort: neuronal spike sorting with Python.
Proc. 7th European Conf. on Python in Science (EuroSciPy'14), pp. 27-34.

Preuss, T., Osei-Bonsu, P.E., Weiss, S.A., Wang, C., and Faber, D.S. (2006). Neural representation of object approach in a decision-making motor circuit. J Neurosci *26*: 3454–3464,

Rind, F.C. (1984). A chemical synapse between two motion detecting neurones in the locust brain. J. Exp. Biol. *110*, 143-167.

Rind, F.C., and Simmons, P.J.. (1992). Orthopteran DCMD neuron: a reevaluation of responses to moving objects. I. Selective responses to approaching objects. J Neurophysiol. *68*, 1654-1666.

Rind, F.C., and Simmons, P.J. (1998). Local circuit for the computation of object approach by an identified visual neuron in the locust. J. Comp. Neurol. *395*, 405-415.

Rowell, C.H.F., O'Shea , M., and Williams, J.L.D. (1977). The neuronal basis of a sensory analyser, the acridid movement detector system. IV. The preference for small field stimuli. J Exp Biol. *68*, 157-85.

Sangaletti, R., Dahl, G., and Bianchi, L. (2014). Mechanosensitive unpaired innexin channels in *C. elegans* touch neurons. Am J Physiol Cell Physiol. *307(10)*, C966-C977.

Schlotterer, G.R. (1977). Response of the locust descending movement detector neuron to rapidly approaching and withdrawing visual stimuli. Can J Zool. *55*,1372–1376.

Sun, H., and Frost, B.J. (1998). Computation of different optical variables of looming objects in pigeon rotundus neurons. Nat Neurosci *1*: 296–303,

Strausfeld, N.J. and Nassel, D.R. (1981). Neuroarchitectures serving compound eyes of crustacea and insects. In: Handbook of Sensory Physiology, vol. VII/7B, edited by Autrum H. Berlin: Springer, pp. 1-132.

Tuthill, J.C., Nern, A., Holtz, S.L., Rubin, G.M., and Reiser, M.B. (2013). Contributions of the 12 neuron classes in the fly lamina to motion vision. Neuron. *79*, 128-140.

von Reyn, C.R., Nern, A., Williamson, W.R., Breads, P., Wu, M., Namiki, S., and Card, G.M. (2017). Feature Integration Drives Probabilistic Behavior in the Drosophila Escape Response. Neuron. *94*, 1190-1204.

Wehr, M., Pezaris, J.S., Sahani, M. (1999). Simultaneous paired intracellular and tetrode recordings for evaluating the performance of spike sorting algorithms. Neurocomputing. *26-27*:1061-1068.

Wu, G.K., Arbuckle, R., Liu, B.H., Tao, H.W., and Zhang, L.I. (2008). Lateral sharpening of cortical frequency tuning by approximately balanced inhibition. Neuron. *58*, 132-143.

Wu, L.Q., Niu, Y.Q., Yang, J., and Wang, S.R. (2005). Tectal neurons signal impending collision of looming objects in the pigeon. Eur. J. Neurosci. *22*, 2325-2331.

Zhu, Y. and Gabbiani, F. (2016). Fine and Distributed Subcellular Retinotopy of Excitatory Inputs to the Dendritic Tree of a Collision-Detecting Neuron. J. Neurophysiol. *115*, 3101–3112.

Zhu, Y., Dewell, B.R., Wang, H., and Gabbiani, F. (2017). Presynaptic Lateral Excitation Mediated by Muscarinic Acetylcholine Receptors Contributes to Object Segmentation in a Collision Detection Circuit. Submitted.

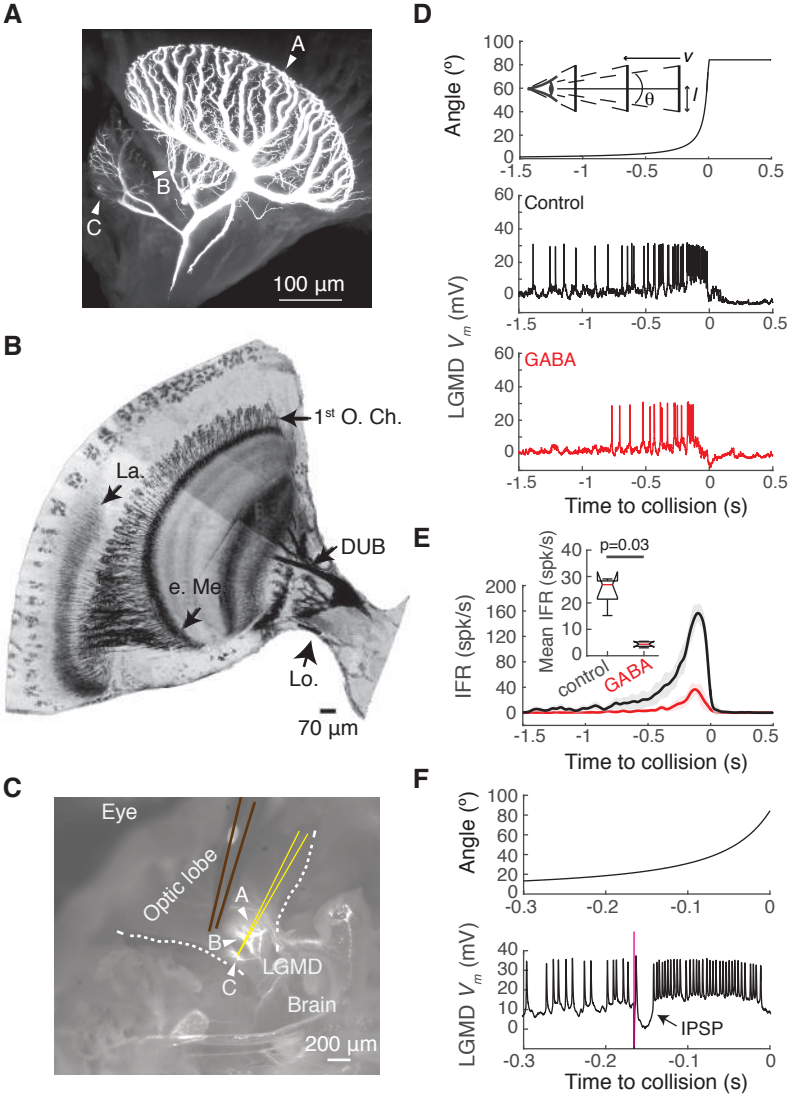

Hongxia et al., Fig. 1

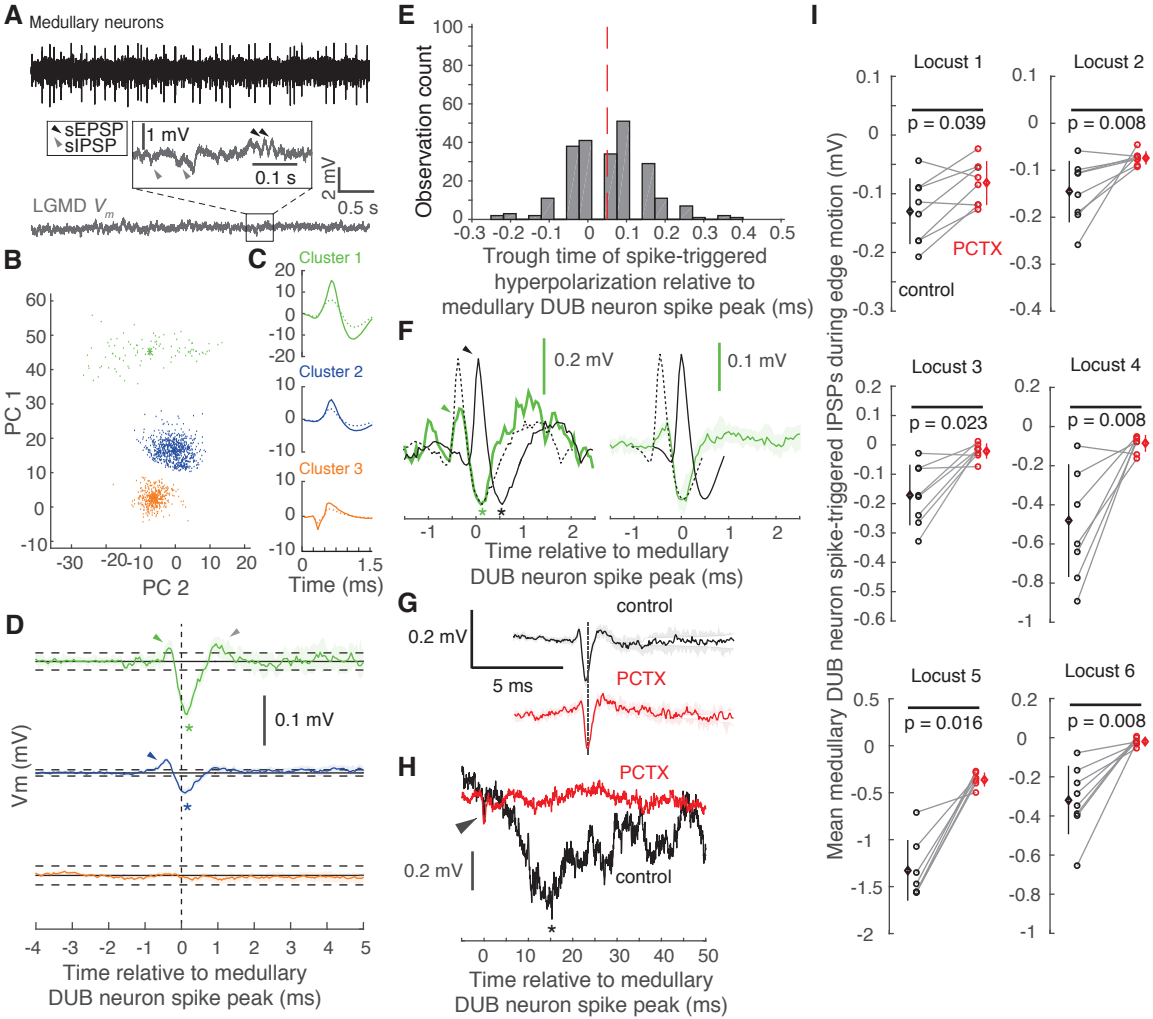

Hongxia et al., Fig. 2

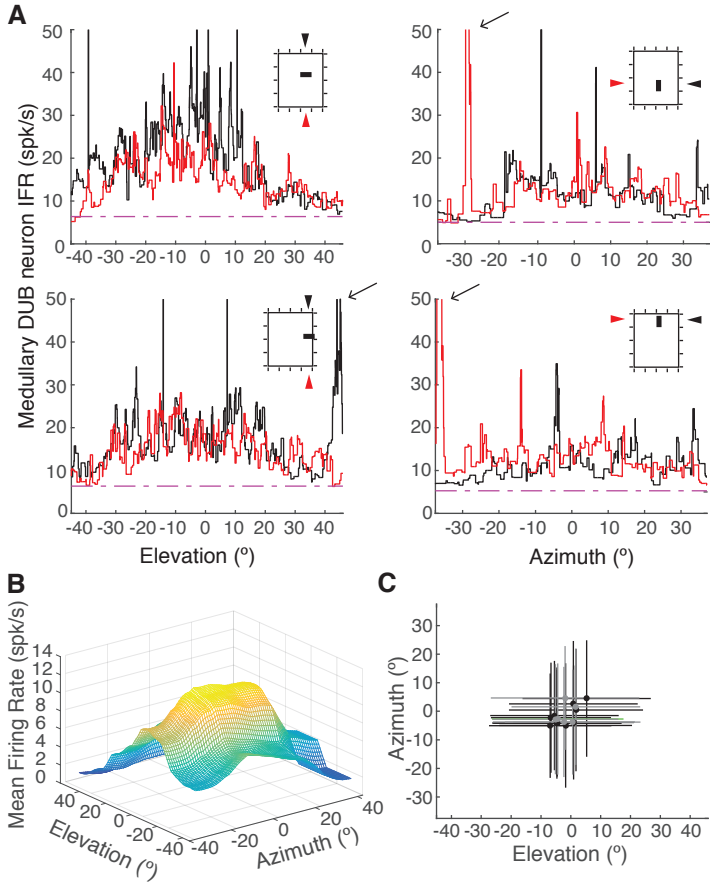

Hongxia et al., Fig. 3

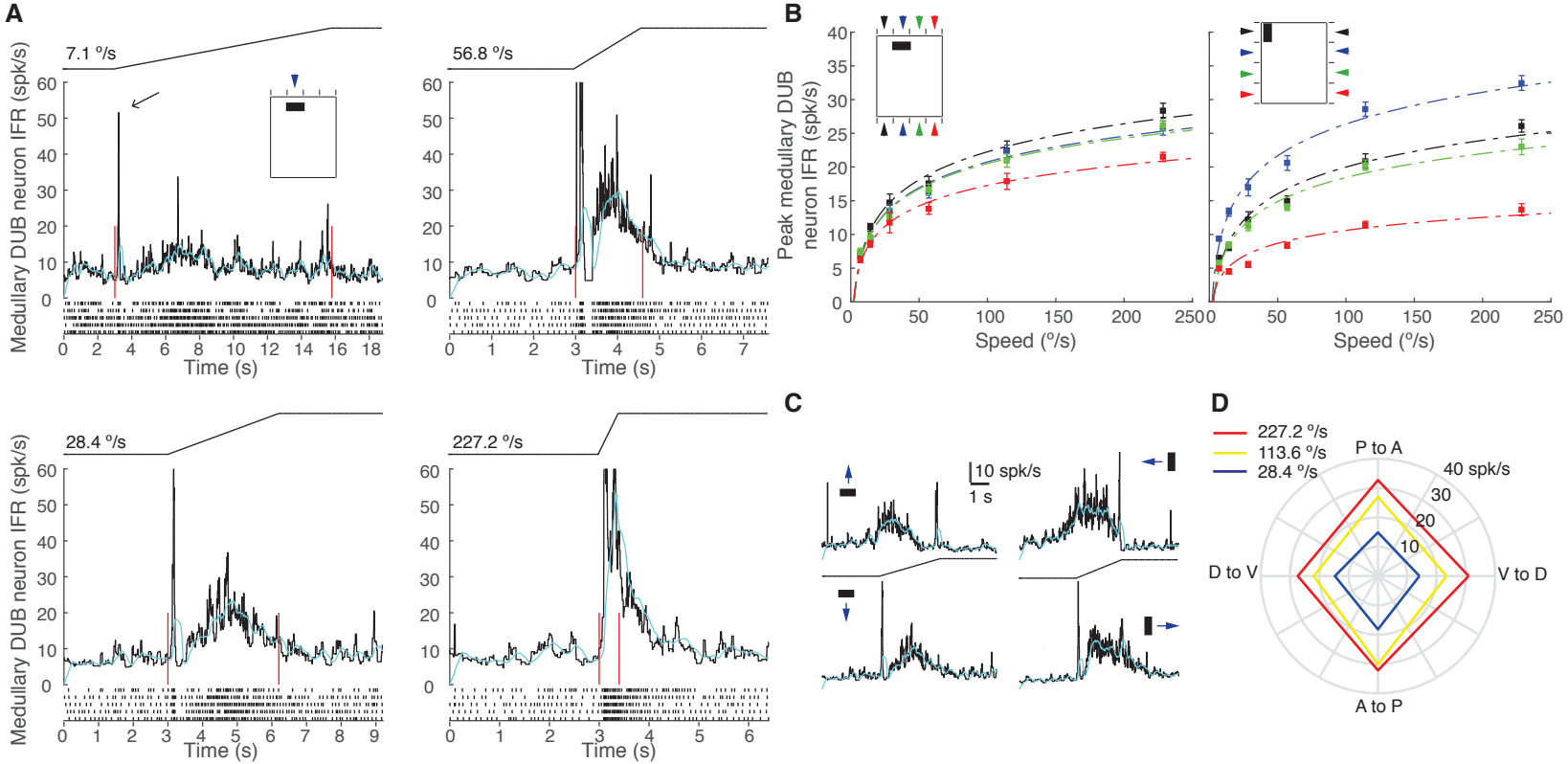

Hongxia et al., Fig. 4

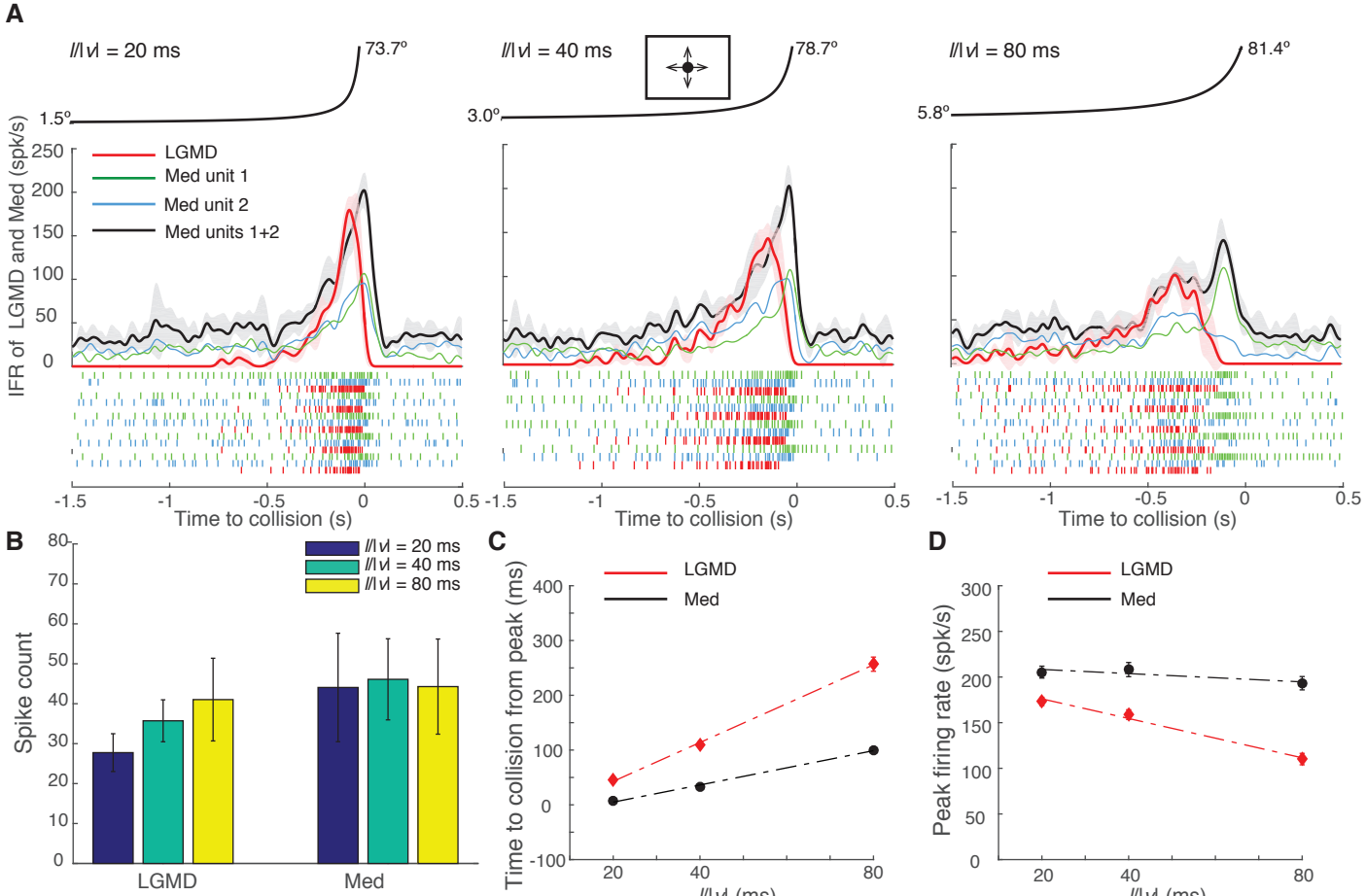

Hongxia et al., Fig. 5

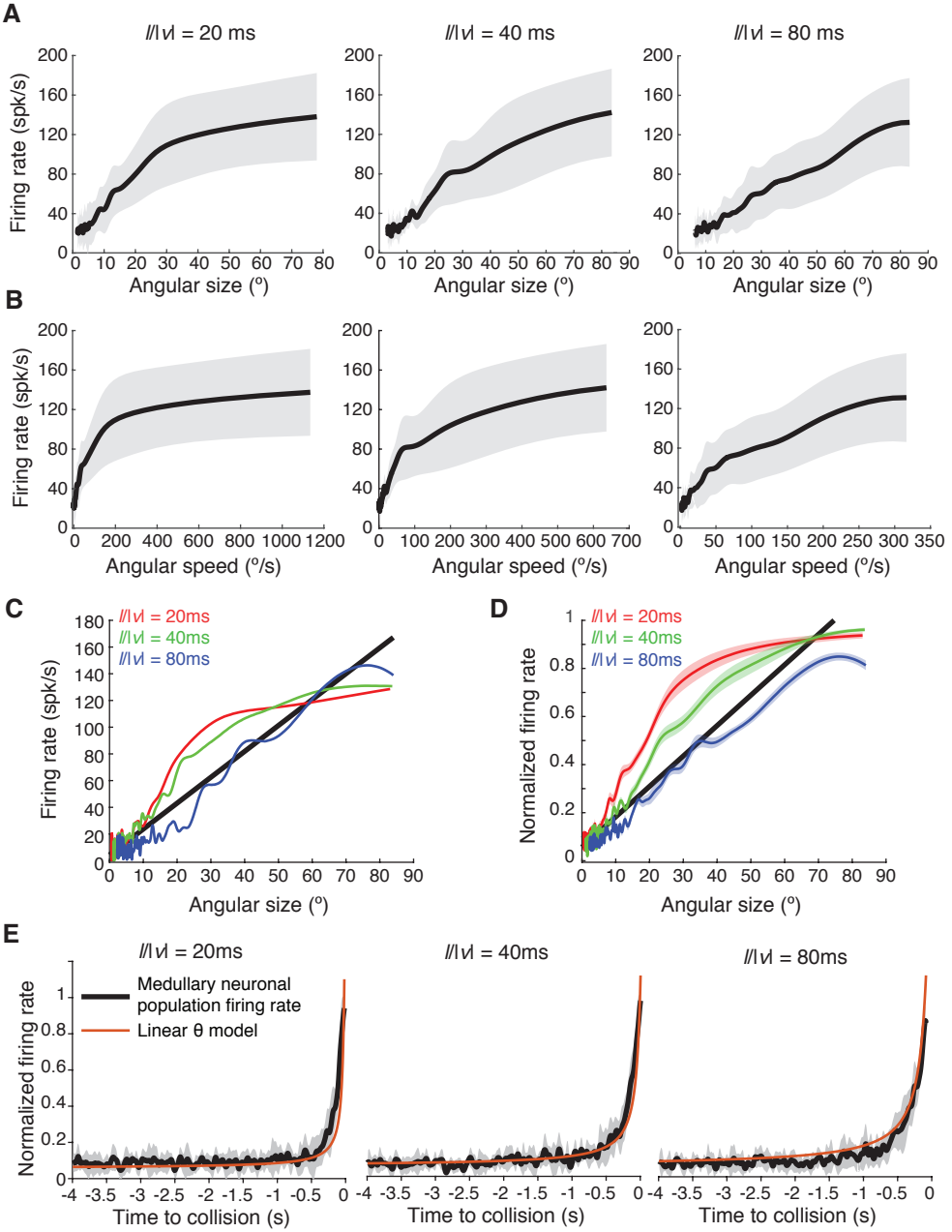

Hongxia et al., Fig. 6

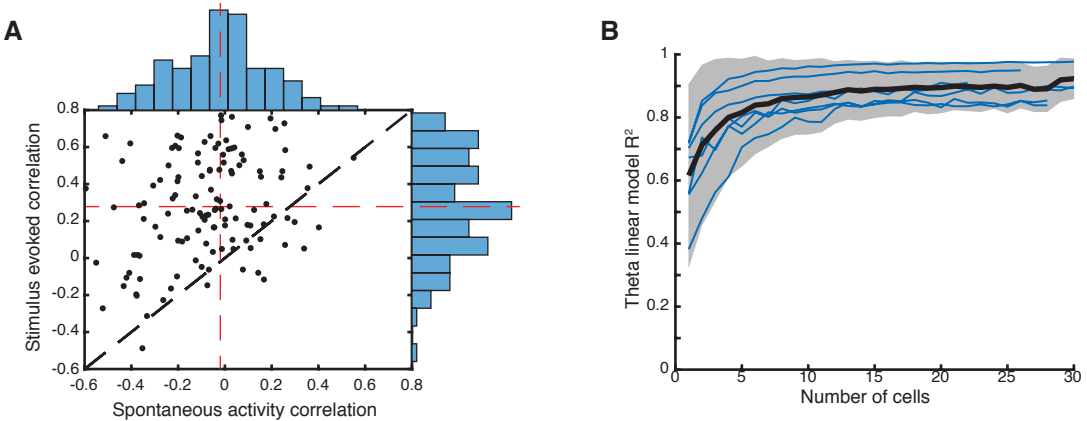

Hongxia et al., Fig. 7